Helical order and multiferroicity in the S = 1/2 quasi-kagome system KCu3As2O7(OD)3

G. J. Nilsen, Y. Okamoto, H. Ishikawa, Virginie Simonet, Claire Colin, Andres Cano, L. C. Chapon, T. Hansen, H. Mutka, Z. Hiroi

PHYSICAL REVIEW B **89**, 140412(R) (2014)

Helical order and multiferroicity in the $S = \frac{1}{2}$ quasi-kagome system $KCu_3As_2O_7(OD)_3$

G. J. Nilsen,[1,2,*] Y. Okamoto,[2] H. Ishikawa,[2] V. Simonet,[3] C. V. Colin,[3] A. Cano,[4] L. C. Chapon,[1] T. Hansen,[1] H. Mutka,[1] and Z. Hiroi[2]

[1]*Institut Laue-Langevin, 6 rue Jules Horowitz, 38042 Grenoble, France*

[2]*Institute for Solid State Physics, University of Tokyo, Kashiwa, Chiba 277-8581, Japan*

[3]*Institut Néel, CNRS and Université Joseph Fourier, 38042 Grenoble, France*

[4]*CNRS, University of Bordeaux, ICMCB, UPR 9048, 33600 Pessac, France*

(Received 26 December 2013; published 28 April 2014)

Several Cu^{2+} hydroxide minerals have been recently identified as candidate realizations of the $S = 1/2$ kagome Heisenberg model. In this context, we have studied the distorted system $KCu_3As_2O_7(OD)_3$ using neutron scattering and bulk measurements. Although the distortion favors magnetic order over a spin liquid ground state, refinement of the magnetic diffraction pattern below $T_{N1} = 7.05(5)$ K yields a complex helical structure with $\mathbf{k} = (0.77,0,0.11)$. This structure, as well as the spin excitation spectrum, are well described by a classical Heisenberg model with ferromagnetic nearest neighbor couplings. Multiferroicity is observed below T_{N1}, with an unusual crossover between improper and pseudoproper behavior occurring at $T_{N2} = 5.5$ K. The polarization at $T = 2$ K is $P = 1.5\ \mu Cm^{-2}$. The properties of $KCu_3As_2O_7(OD)_3$ highlight the variety of physics which arise from the interplay of spin and orbital degrees of freedom in Cu^{2+} kagome systems.

DOI: 10.1103/PhysRevB.89.140412 PACS number(s): 75.85.+t, 75.10.Hk, 75.10.Jm, 75.25.−j

The ground state of the highly frustrated $S = 1/2$ kagome lattice Heisenberg model has inspired considerable debate over the past 20 years, with recent theoretical candidates including exotic gapped $\mathcal{Z}_2$ [1] and gapless $U(1)$ [2] spin liquid states. This has motivated an extensive search for potential realizations, which has thus far focused on Cu^{2+}-containing minerals, where the kagome lattices are made up of edge-sharing CuO_6 octahedra. A wide range of interesting magnetic behaviors have been observed in this family of materials; in herbertsmithite ($R\bar{3}m$) [3], no magnetic order and only short range dynamical correlations are found down to low T [4–6], while for volborthite ($C2/m$) [7–10], incommensurate long range order is only observed around 1 K, despite $\theta_{CW} = -115$ K. In kapellasite [11], a polymorph of herbertsmithite, an unusual noncoplanar spin liquid is found to be promoted by disorder and further neighbor couplings [12]. Numerous attempts have been made to understand this diversity theoretically; a symmetry analysis of the further neighbor Heisenberg model, for example, has identified three possible coplanar and five noncoplanar commensurate magnetically ordered ground states [13]. Exact diagonalizations of finite clusters show that asymmetric exchange favors commensurate long range order [14,15], while depletion of the kagome lattice is understood to lead to a valence bond glass [16].

The present Rapid Communication focuses on the recently uncovered synthetic Cu^{2+}-based mineral $KCu_3As_2O_7(OD)_3$ [17], which, as volborthite, is monoclinically distorted. Elastic and inelastic neutron scattering are used to probe the unusual incommensurate magnetic ground state of $KCu_3As_2O_7(OD)_3$. When combined with dielectric constant and polarization measurements, these show that $KCu_3As_2O_7(OD)_3$ is a rare realization of a kagome lattice multiferroic.

$KCu_3As_2O_7(OD)_3$ crystallizes in the $C2/m$ space group, with lattice parameters $a = 10.287$ Å, $b = 5.972$ Å, $c = 7.849$ Å, and $\beta = 117.74°$ [18]. There are two crystallographically inequivalent Cu^{2+} sites: Cu1 at (0,0,0) (Wyckoff position $2a$) and Cu2 at (1/4,1/4,0) ($4e$). The CuO_6 octahedra share edges in the ab plane, forming a distorted kagome lattice (Fig. 1). An analysis of the distortions of the CuO_6 octahedra [17] results in the assignment of $d_{x^2-y^2}$ as the magnetically active orbital on the Cu2 site, with d_{z^2} singly occupied on Cu1. There are thus two types of nearest neighbor superexchange: Neighboring Cu1 and Cu2 sites are connected by O4 in the μ_3 bridging mode, with $\angle$Cu-O-Cu $= 101.9°$ and a Cu-Cu distance $r_{\text{Cu-Cu}}$ of 2.97 Å. The link between adjacent Cu2 is formed by the same O4, but with a slightly smaller $\angle$Cu-O-Cu$= 101.4°$ and longer $r_{\text{Cu-Cu}} = 2.99$ Å. The exchange constants belonging to these pathways are referred to as J and J', respectively (note the difference between this definition and that in Ref. [17]).

In the conventional picture of superexchange across a μ_2-bridging anion, the sign of J is related to $\angle$Cu-O-Cu. For μ_3-bridged Cu triangles, however, it is found that the sign is determined by the distance between μ_3-O (here O4) and the plane of the Cu triangle (here ΔCu2-Cu2-Cu1), r(O-Cu$_3$) [19]. In $KCu_3As_2O_7(OD)_3$, r(O-Cu$_3$) $= 0.85$ Å, considerably in excess of the $r_c = 0.35$ Å beyond which a ferromagnetic J is expected. Indeed, a Curie-Weiss fit of the high temperature susceptibility yields a ferromagnetic Weiss constant $\theta_{CW} \sim 14$ K ~ 1.2 meV [17]. On the other hand, r(O-Cu$_3$) $> r_c$ also in vesignieite [20], where $\theta_{CW} < 0$. Unambiguous assignment of the sign of superexchange based on structural parameters is therefore difficult in these materials. At lower temperatures, magnetic long range order is found to occur in $KCu_3As_2O_7(OD)_3$ at $T_{N1} = 7.1$ K, as indicated by a kink in $\chi(T)$ and a sharp anomaly in the specific heat $C_p(T)$. In addition, a shoulder is observed in the specific heat at $T_{N2} \simeq 5.5$ K, which we will later show to be another magnetic transition [17].

A deuterated sample suitable for neutron scattering experiments was synthesized by performing the previously

*nilsen@ill.fr

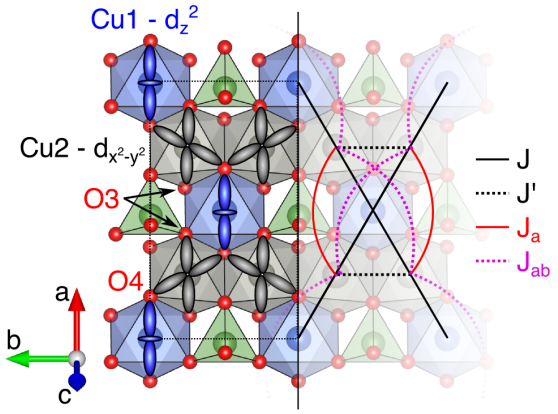

FIG. 1. (Color online) Left: Structure and assumed orbital ordering pattern for $KCu_3As_2O_7(OD)_3$. The kagome lattice, a two-dimensional network of corner-sharing triangles, is formed by edge-sharing Cu1 (blue) and Cu2 (black) octahedra. Right: Magnetic exchange paths used in Eq. (1).

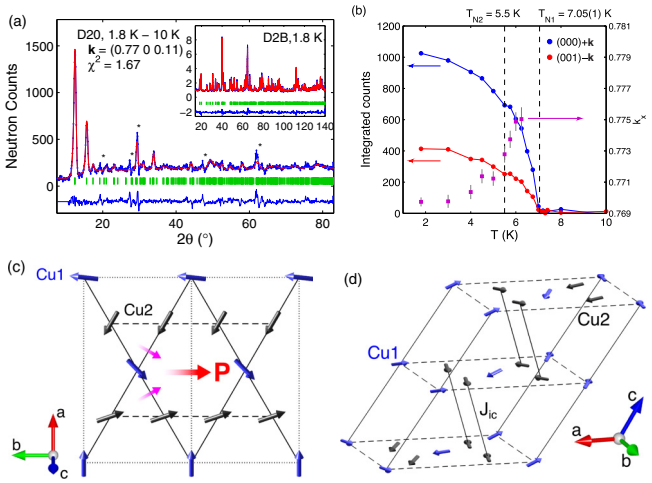

FIG. 2. (Color online) (a) Subtracted elastic neutron scattering spectra (blue dots) from D20 with Rietveld refinement (red line) of the magnetic structure. The oscillations around nuclear Bragg positions (*) are an artifact resulting from the Debye-Waller factor. Inset: Rietveld refinement of the nuclear structure from high-resolution D2B data. (b) Magnetic intensity vs T for the $(000)+\mathbf{k}$ and $(001)-\mathbf{k}$ reflections. The transitions observed in specific heat measurements are marked by dashed vertical lines. (c) The refined magnetic structure viewed along $\mathbf{c}^*$. The red and pink arrows indicate the total polarization and contributions to it from the $\langle 110\rangle$ chains, respectively. (d) The propagation of the magnetic structure along c. Note the antiparallel alignment of spins related by the centering translation on adjacent planes. The Cu-Cu pathway between these is also the shortest, and is thus assigned to J_{ic}.

reported synthesis in D_2O rather than H_2O solvent [17]. All operations were carried out in a dry atmosphere to avoid exchange between D and H, and the sample purity was verified by both x-ray diffraction and superconducting quantum interference device (SQUID) magnetometry. Around 5 g of the powder sample was loaded in a 9 mm V can, and cooled to temperatures down to 1.8 K using a standard ^{4}He Orange cryostat. Neutron diffraction patterns were collected on the D20 instrument at ILL using $\lambda = 2.41$ Å neutrons from a PG(002) monochromator at a takeoff angle $\theta = 42^\circ$; these conditions optimize flux at the expense of resolution. The background from the sample environment was reduced using a radial oscillating collimator, and spectra were collected at $T = 1.8 < T_N < 10$ K. Higher resolution patterns for the determination of the nuclear structure were measured at $T = 1.8$ K on D2B (ILL), using $\lambda = 1.594$ Å from the (335) reflection of a Ge monochromator with $\theta = 135^\circ$. Inelastic neutron scattering data were collected at the IN4 (ILL) time-of-flight spectrometer with an incident energy $E_i = 9.2$ meV ($\lambda = 2.981$ Å). Measurements of the dielectric constant ϵ_r were carried out on a pressed pellet of thickness $d = 0.65$ mm silver pasted to flat electrodes, and connected to an *LCR* meter (Agilent E4980A). Finally, the polarization P was determined by integrating the pyroelectric current measured on the same pellet using an electrometer (Keithley 6517A), cooling in electric fields of ± 307 kV m^{-1}.

We begin the discussion of our results by establishing the nuclear structure; a Rietveld refinement of the high-resolution diffraction data yields lattice parameters $a = 10.2872(1)$ Å, $b = 5.9728(1)$ Å, $c = 7.8492(1)$ Å, and $\beta = 117.740(1)^\circ$, which agree well with those reported in Ref. [18]. The H/D atoms are placed based on symmetry considerations, and refinement yields coordinates (0.261(1),0,0.265(1)) for H1 and (0.5,0,0.5) for H2, respectively. H2 forms a hydrogen bond along with two O2 atoms belonging to adjacent AsO_4 groups. The deuteration was estimated to be 96.0(2)% on the H1 site and 84(2)% on H2.

In the medium-resolution D20 data, several magnetic Bragg peaks are observed below $T_{N1} = 7.05(5)$ K, all of which may be uniquely indexed by the incommensurate $\mathbf{k}$ vector = (0.7750(4),0,0.1090(4)) at $T = 6.25$ K. Cooling further, k_x (k_z) decreases (increases), saturating at $\mathbf{k} =$ (0.7697(1),0,0.1109(1)) at 1.8 K [Fig. 2(b)]. Around $T_{N2} =$ 5.5 K, there is a discontinuity in the intensities of the $(000)+\mathbf{k}$ and $(001)-\mathbf{k}$ Bragg peaks, and an accompanying small shift in their relative intensity. This overall temperature dependence is compatible with the thermodynamic data [17]. As no additional Bragg peaks are observed below T_{N2}, the subtle difference in magnetic structure between $T_{N2} < T < T_{N1}$ and $T < T_{N2}$ is not distinguishable in the present study. Accordingly, we focus on the $T = 1.8$ K $< T_{N2}$ data for the subsequent analysis of the magnetic structure.

Because the experimentally determined $\mathbf{k}$ vector does not coincide with a high symmetry point in the Brillouin zone, a full description of the magnetic symmetry requires determining the irreducible corepresentations of the magnetic group $\mathbf{M} = \mathbf{G}^k + K\mathbf{h}$, where $\mathbf{S} = \{E, m_y, 2_y, \bar{1}\}$ is the space group, $\mathbf{G^k} = \{E, m\}$ is the little group of operators leaving $\mathbf{k}$ invariant, $\mathbf{h} = \mathbf{S} - \mathbf{G^k}$, and K is the complex conjugation operator [21]. We thus find two one-dimensional real coreps, D_1 and D_2, for which the basis functions ψ_α may be calculated by the usual projection method. The D_1 mode has the spins on the Cu1 site pointing in the b direction, with the a and c components antiparallel between the two orbits of the Cu2 site (Table I). For the D_2 mode, on the other hand, the magnetic moment on the Cu1 site lies in the ac plane, while the b components of the Cu2 spins are antiparallel.

TABLE I. Characters and basis functions ψ_α of the corepresentations of the magnetic group **M**. The Cu2 site is split into two orbits, with Cu2′ at (1/4,3/4,0).

Corep/Irrep	$E\ K\bar{1}$	$2_y\ Km_y$	ψ_{Cu1}	ψ_{Cu2}	$\psi_{Cu2'}$
D_1/Γ_1	1	1	(0,1,0)	(1,1,1)	(−1,1,−1)
D_2/Γ_2	1	−1	(1,0,1)	(1,1,1)	(1,−1,1)

Fitting the magnetic scattering $I_{mag} = I(1.8\ K) - I(10\ K)$ to either of the above modes individually yields poor agreement with the experimental data; $\chi^2 > 4$ in both cases. We must therefore shift our attention to solutions involving both. Considering only solutions where the modes are summed in quadrature and recalling that the elements of **h** complex conjugate the basis functions, two possible types of state result: a helix with point group $21'$ for $D_1 + iD_2$ $(iD_1 + D_2)$ and an amplitude modulated structure with point group $m1'$ for $D_1 + iD_1$ $(D_2 + iD_2)$. Because the structure is defined by a single **k** vector, we employ the refinement constraint that the spins on either sublattice must be coplanar. In addition, for the helical $D_1 + iD_2$-type structure, we restrict the envelope of the helix to being circular by refining the spherical components (μ,θ,ϕ) of the Fourier coefficients in the $A2/m$ setting of the space group ($a' = c$, $b' = a$, $c' = b$). We note that the point groups of both possible solutions are polar, and therefore compatible with ferroelectricity.

The best fit ($\chi^2 = 1.67$) is achieved for the $iD_1 + D_2$ solution, with the plane of the helix rotated out of the ac plane by the azimuthal angle $\phi_{Cu1} = \phi_{Cu2} = 148(2)^\circ$ and the polar angle $\theta_{Cu1} = \theta_{Cu2} = 166(5)^\circ$. The Cu2 ($4e$) site is split into two orbits with the same phase $\phi_{Cu2} = \phi_{Cu2'} = k_x/4 = 0.1923$ [Fig. 2(a)]. The ordered moments are found to be $0.86(2)\mu_B$ for Cu1 and $0.87(1)\mu_B$ for Cu2, close to the full $1\mu_B$ expected for Cu^{2+}, suggesting a surprisingly small fluctuating component for a frustrated quantum spin system. The magnetic structure may be described as crossing helical chains along the ⟨110⟩ directions, with ferromagnetic alignment along the b direction [Fig. 2(c)]. Along c, the moment direction is slowly modulated, with a period of approximately 10 unit cells [Fig. 2(d)]. Spins related to each other by the centering translation are antiparallel on adjacent layers, i.e., $\mathbf{m}(1/4,1/4,0) = -\mathbf{m}(3/4,1/4,1)$. Finally, the plane of rotation for both sites is tilted out of the ab plane by $31(2)^\circ$.

Next, we seek a microscopic model that explains the refined magnetic structure. It is clear that the nearest neighbor Heisenberg Hamiltonian on the kagome lattice is insufficient for this purpose. As such, the presence of either further neighbor couplings or anisotropic terms in the Hamiltonian is required. We identify two likely further neighbor superexchange pathways within the kagome planes: one between Cu2 atoms along the ⟨100⟩ direction, mediated by two O3 atoms (Fig. 1), with $2(\angle\text{Cu-O-O}) = 187.2^\circ$ and $r(\text{Cu-Cu}) = 5.12$ Å, and the other along ⟨110⟩ through O3 and O4, with $2(\angle\text{Cu-O-O}) = 291.8^\circ$. The latter is similar to the pathway which yields antiferromagnetic next nearest neighbor exchange in edge-shared square planar Cu^{2+} systems such as $LiCuVO_4$ [22] and $CuGeO_3$ [23]. The exchange integrals corresponding to the two pathways above will be referred to as J_a and J_{ab}, respectively. If $J_a > 0$, as seems likely

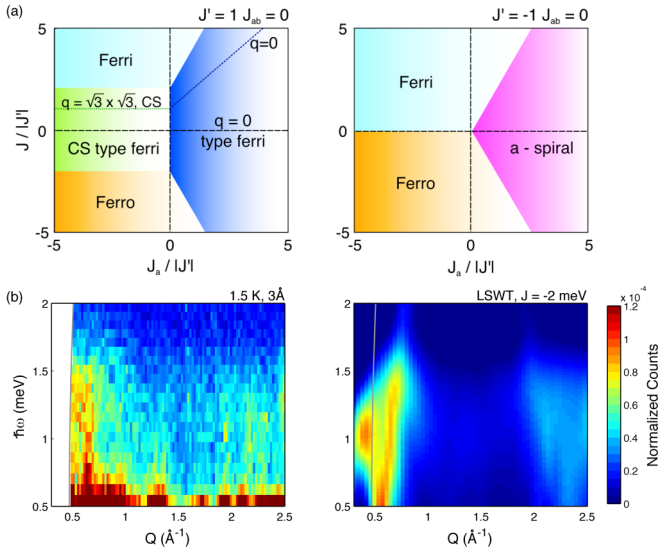

FIG. 3. (Color online) (a) Phase diagrams in the $J' = 1$ and $J' = -1$ planes derived by solving Eq. (1) subject to Eq. (2). When $J' < 0$, a large area is occupied by the experimentally observed a-helical phase. (b) Comparison of linear spin wave theory (right) and inelastic neutron scattering data (left) for the parameters listed in the text.

from $\angle$Cu-O-O-Cu $\sim 180^\circ$, it frustrates the nearest neighbor coupling J when $J < 0$ (Fig. 1). Likewise, for $J_{ab} > 0$, frustration arises when $J' < 0$. An interplane coupling is also required to explain the modulation along the c direction; the only plausible pathway is through the AsO_4 tetrahedra, which are joined by H2. The simplest model which can be constructed for Heisenberg spins is then

$$\mathcal{H} = \sum_{i,j} J(|\mathbf{r}_i - \mathbf{r}_j|)\mathbf{S}_i \cdot \mathbf{S}_j, \qquad (1)$$

where the sum is over all pairs of classical unit spins $\mathbf{S}_{i,j}$ at $\mathbf{r}_{i,j}$ which are connected by $J(|\mathbf{r}_i - \mathbf{r}_j|)$.

Since the experimentally determined structure is a coplanar helix, the spin on each sublattice may be written as

$$\mathbf{S}_i^\alpha = S[\hat{x}\cos(\mathbf{k}\cdot\mathbf{r}_i + \phi_\alpha) - \hat{y}\sin(\mathbf{k}\cdot\mathbf{r}_i + \phi_\alpha)], \qquad (2)$$

where $\hat{x}$ and $\hat{y}$ are unit vectors along a and b, and ϕ_α is the phase on sublattice α. Setting $J_{ab} = 0$, $J' = \pm 1$, $J_{ic} = 0.01$, and minimizing with respect to **k** and ϕ_α, we thus arrive at the phase diagrams shown in Fig. 3(a). In the $J' = 1$ plane, there are, in addition to the trivial ferromagnetic and Néel ferrimagnetic states, two tilted ferrimagnetic states interpolating between them, as well as narrow strips of uniform ($\mathbf{q} = 0$), striped (CS), and staggered chirality order ($\mathbf{q} = \sqrt{3} \times \sqrt{3}$). For $J' = -1$, the phase diagram is considerably simpler, and for antiferromagnetic J_a, the experimentally observed a helix is found. The components of the **k** vector in this state are found to be $k_x = 2 - 2/\pi[\cos^{-1}(|J|/J_a)]$ and $k_z = (1 - k_x)/2$ for antiferromagnetic J_{ic}. The experimental **k** is thus accurately reproduced for the condition $|J| \sim 0.68J_a$, for $J, J' < 0$; when J_{ab} is included, the right side of the previous expression becomes $0.68(J_a + J_{ab})$.

To gain a more quantitative grasp of the magnitudes of $J(|\mathbf{r}_i - \mathbf{r}_j|)$, we proceed to calculate the linear spin wave spectrum for comparison with $S(Q,\hbar\omega)$ collected in the

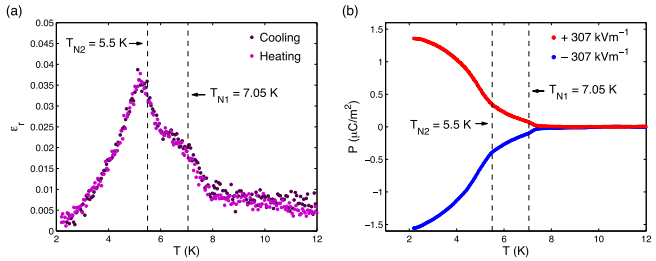

FIG. 4. (Color online) (a) The temperature dependence of the dielectric constant ϵ_r measured at 10 kHz with $V_{ac} = 1$ V. A linear background has been subtracted for clarity. Anomalies are observed at both T_{N1} and T_S. (b) The polarization P vs temperature. The red (blue) curve corresponds to a sample poled in an electric field of $+307$ (-307) kV m^{-1}. In both panels, the features observed by other probes at T_{N1} and T_S are marked by dashed vertical lines.

ordered phase on the inelastic neutron spectrometer IN4 (Fig. 3). In addition to the requirement determined above, another constraint on $J(|\mathbf{r}_i - \mathbf{r}_j|)$ arises from the Weiss constant $\theta_{\rm CW} = -(4k_B)^{-1} \sum_{i=1}^{z} z_i J_i \sim 1.3$ meV. Solutions with both ferromagnetic and antiferromagnetic J were calculated, but only those with both J and J' ferromagnetic are able to generate the correct bandwidth while simultaneously giving a reasonable $\theta_{\rm CW}$. In addition, $J_a > J_{ab}$ is required to reproduce the reduction in intensity above $\hbar\omega = 1.5$ meV. The powder averaged $S(Q,\hbar\omega)$ for the following parameter set is shown in Fig. 3(b): $J = -2$ meV, $J' = -1$ meV, $J_{ab} = 0.75$ meV, $J_a = 2.2$ meV, $J_{ic} = 0.01$ meV. Beyond the good qualitative agreement with experiment, this solution gives an ordered moment $\sim 0.8\mu_B$ on both sites, consistent with the refined moment.

While the further-neighbor Heisenberg model proposed above has thus far been successful in describing our experimental data, it should be noted that Dzyaloshinskii-Moriya (DM) couplings are also allowed in $KCu_3As_2O_7(OD)_3$. Their presence is an important difference with respect to other helical magnets, such as $LiCuVO_4$, where this type of interaction is forbidden by symmetry [24]. Given that DM terms favor orthogonal alignment of spins, and therefore alter the pitch angle of the helix, their experimental determination is particularly important.

We finally move on to the magnetoelectric properties of $KCu_3As_2O_7(OD)_3$; according to the $21'$ point-group symmetry of the low-temperature helical magnetic structure, an electric polarization is anticipated along the b direction. Indeed, we observe a switchable spontaneous polarization approaching $P \sim 1.5\ \mu$Cm^{-2} at 2 K, which is compatible with ferroelectricity of a magnetic origin [25]. The temperature dependence of this polarization reveals a number of remarkable features: First, P becomes nonzero at T_{N1}, below which it increases linearly [Fig. 4(b)]. This, along with the steplike anomaly in ϵ_p at T_{N1} [Fig. 3(a)], is a hallmark of improper ferroelectricity, as originally defined in Ref. [26]. The linear T dependence reveals a coupling $P\eta^2$ with the primary order parameter η associated with the magnetic order [27]. At T_{N2}, a transformation to more conventional (pseudoproper) ferroelectric behavior is observed, with a divergent dielectric constant and a square-root behavior for the electric polarization. This change is absent in model spin-driven ferroelectrics such as $TbMnO_3$ [28] and $TbMn_2O_5$ [29], which display only the pseudoproper regime [30,31]. The striking concurrence of ferroelectricity with magnetic ordering and its transformation from improper to pseudoproper suggests that the multiferroic interplay in kagome systems is both complex and rich. Its understanding requires a more precise characterization of the order that appears below T_{N1}, which will be reported elsewhere.

In conclusion, we have carried out elastic and inelastic neutron scattering experiments, as well as dielectric and polarization measurements on the quasi-kagome $S = 1/2$ quantum magnet $KCu_3As_2O_7(OD)_3$, These experiments convincingly reveal (i) helical magnetic order with an incommensurate propagation vector $\mathbf{k} = (0.77,0,0.11)$ and (ii) well-defined spin-wave excitations, both explained by a Heisenberg exchange model. In addition, the system displays (iii) spin-driven ferroelectricity that appears at the onset of magnetic order and transforms from improper to pseudoproper at lower temperatures.

We thank Sándor Tóth for useful discussions on the spin wave simulations and for sharing the SPINW code [32], Ludovic Gendrin and Stéphane Rols for support during the neutron experiments, and F. Gay for his help in developing the dielectric measurements setup. G.J.N. is grateful to the ISSP for support during the writing of this article.

[1] S. Yan, D. A. Huse, and S. R. White, Science **332**, 1173 (2011).
[2] Y. Iqbal, F. Becca, S. Sorella, and D. Poilblanc, Phys. Rev. B **87**, 060405 (2013).
[3] M. Shores, E. Nytko, B. Bartlett, and D. Nocera, J. Am. Chem. Soc. **127**, 13462 (2005).
[4] J. S. Helton, K. Matan, M. P. Shores, E. A. Nytko, B. M. Bartlett, Y. Yoshida, Y. Takano, A. Suslov, Y. Qiu, J. H. Chung, D. G. Nocera, and Y. S. Lee, Phys. Rev. Lett. **98**, 107204 (2007).
[5] T.-H. Han, J. S. Helton, S. Chu, D. G. Nocera, J. A. Rodriguez-Rivera, C. Broholm, and Y. S. Lee, Nature (London) **492**, 406 (2012).
[6] M. A. de Vries, J. R. Stewart, P. P. Deen, J. O. Piatek, G. J. Nilsen, H. M. Rønnow, and A. Harrison, Phys. Rev. Lett. **103**, 237201 (2009).
[7] Z. Hiroi, M. Hanawa, N. Kobayashi, M. Nohara, H. Takagi, Y. Kato, and M. Takigawa, J. Phys. Soc. Jpn. **70**, 3377 (2001).
[8] M. Yoshida, M. Takigawa, H. Yoshida, Y. Okamoto, and Z. Hiroi, Phys. Rev. Lett. **103**, 077207 (2009).
[9] G. J. Nilsen, F. C. Coomer, M. A. de Vries, J. R. Stewart, P. Deen, A. Harrison, and H. M. Rønnow, Phys. Rev. B **84**, 172401 (2011).

[10] H. Yoshida, J.-i. Yamaura, M. Isobe, Y. Okamoto, G. J. Nilsen, and Z. Hiroi, Nat. Commun. **3**, 860 (2012).
[11] R. H. Colman, C. Ritter, and A. S. Wills, Chem. Mater. **20**, 6897 (2008).
[12] B. Fåk, E. Kermarrec, L. Messio, B. Bernu, C. Lhuillier, F. Bert, P. Mendels, B. Koteswararao, F. Bouquet, J. Ollivier, A. D. Hillier, A. Amato, R. H. Colman, and A. S. Wills, Phys. Rev. Lett. **109**, 037208 (2012).
[13] L. Messio, C. Lhuillier, and G. Misguich, Phys. Rev. B **83**, 184401 (2011).
[14] O. Cepas, C. M. Fong, P. W. Leung, and C. Lhuillier, Phys. Rev. B **78**, 140405 (2008).
[15] I. Rousochatzakis, S. R. Manmana, A. M. Lauchli, B. Normand, and F. Mila, Phys. Rev. B **79**, 214415 (2009).
[16] R. R. P. Singh, Phys. Rev. Lett. **104**, 177203 (2010).
[17] Y. Okamoto, H. Ishikawa, G. J. Nilsen, and Z. Hiroi, J. Phys. Soc. Jpn. **81**, 033707 (2012).
[18] H. Effenberger, Z. Kristallogr. **188**, 43 (1989).
[19] J. Yoon and E. I. Solomon, Inorg. Chem. **44**, 8076 (2005).
[20] Y. Okamoto, H. Yoshida, and Z. Hiroi, J. Phys. Soc. Jpn. **78**, 033701 (2009).
[21] P. G. Radaelli and L. C. Chapon, Phys. Rev. B **76**, 054428 (2007).
[22] M. Enderle, C. Mukherjee, B. Fåk, R. K. Kremer, J. M. Broto, H. Rosner, S. L. Drechsler, J. Richter, J. Malek, A. Prokofiev, W. Assmus, S. Pujol, J. L. Raggazzoni, H. Rakoto, M. Rheinstadter, and H. M. Ronnow, Europhys. Lett. **70**, 237 (2005).
[23] M. Hase, I. Terasaki, and K. Uchinokura, Phys. Rev. Lett. **70**, 3651 (1993).
[24] M. Mourigal, M. Enderle, R. K. Kremer, J. M. Law, and B. Fåk, Phys. Rev. B **83**, 100409 (2011).
[25] S.-W. Cheong and M. Mostovoy, Nat. Mater. **6**, 13 (2007).
[26] A. P. Levanyuk and D. G. Sannikov, Sov. Phys. Usp. **17**, 199 (1974).
[27] We note that neither corep D_1 nor D_2 are polar. The ferrolectricity observed below T_{N1} thus implies that both participate in the magnetic ordering and, consequently, that the transition should be discontinuous. This is in contradiction with the second-order transitions observed experimentally [Figs. 2(b) and 4], which suggests that spin-orbit coupling is marginal and the transitions are better described within the exchange approximation. In this case, the order parameter belongs to the exchange multiplet $\eta = D_1 + 2D_2$ of representations that remain invariant under spin rotation [33].
[28] T. Kimura, T. Goto, H. Shintani, K. Ishizaka, T. Arima, and Y. Tokura, Nature (London) **426**, 55 (2003).
[29] N. Hur, S. Park, P. A. Sharma, J. S. Ahn, S. Guha, and S.-W. Cheong, Nature (London) **429**, 392 (2004).
[30] P. Tolédano, Phys. Rev. B **79**, 094416 (2009).
[31] A. Cano and A. P. Levanyuk, Phys. Rev. B **81**, 172105 (2010).
[32] S. Tóth and B. Lake, arXiv:1402.6069 [cond-mat].
[33] Y. A. Izyumov, V. E. Naish, and S. B. Petrov, J. Magn. Magn. Mater. **13**, 275 (1979).